Mechanical Systems and Signal Processing 217 (2024) 111540

Contents lists available at ScienceDirect

Mechanical Systems and Signal Processing

journal homepage: www.elsevier.com/locate/ymssp

Mechanical overload protection strategies for energy harvesters with frequency up-conversion mechanism

Guansong Shan, Dong Wang *, Meiling Zhu *

Faculty of Environment, Science and Economy, University of Exeter, Exeter, UK

ARTICLE INFO

Communicated by: Daniil Yurchenko

Keywords:
Vibration energy harvesting
Frequency up-conversion mechanism
Mechanical overload protection
Reliability
FEM simulation

ABSTRACT

Vibration energy harvesters utilising the frequency up-conversion mechanism have been effective in harvesting low-frequency ambient vibrations. However, the mechanical impact required for this process could also damage the devices when excessive load is applied. To address this issue, this paper presents novel protection strategies for energy harvesters with a frequency up-conversion mechanism, including a ring-type stopper within the resonant system and specially designed impact protection components (IPC) within the impact system. By applying these methods, the influence of excessive input excitation has been mitigated, and thus, the reliability and durability of the device have been improved. Finite element modelling has been employed to model the proposed protection methods, and then experiments have been conducted to verify and refine the modelling. Stress analysis is finally conducted based on the refined model to validate the effectiveness of the protection strategies. The results demonstrate that the proposed strategies are capable of protecting the harvesting system from excessive input excitations, which means the device functions effectively in the operating state and decelerates the growth rate of maximum stress and acceleration in the limiting state. This research contributes valuable insights into the development of effective protection strategies for energy harvesters with frequency up-conversion mechanisms, thereby improving their durability and performances in real-world applications.

1. Introduction

Vibration energy harvesters, which convert ambient vibrations into electrical energy, have demonstrated significant potential as power sources. However, while these vibrations are crucial for the operation of these harvesters, they also pose a potential threat to the integrity of the system. The inherently random vibrations from sources like railway tracks [1], bridges [2], and roads [3] generate a wide range of acceleration variations. This induces a design challenge for energy harvesters capable of withstanding such intense vibrations. As a result, it is essential to incorporate mechanical overload protection strategies to secure these devices against potential damage.

Current methods for protecting against mechanical overload primarily focus on resonant energy harvesters. While optimising the cross-section of the cantilever structure and operating in compressive strain can reduce the maximum strain, limiting the amplitude of the inertial mass movement is a more effective means of mechanical overload protection [4]. Kim et al. [5] discovered that sudden overloads were the primary cause of failure in vibration energy harvesters through an analysis of the failure mode of a harvester that had malfunctioned during a vibration test. To mitigate this, a mechanical stopper was implemented on an electromagnetic energy

* Corresponding authors.
E-mail addresses: d.wang2@exeter.ac.uk (D. Wang), m.zhu@exeter.ac.uk (M. Zhu).

https://doi.org/10.1016/j.ymssp.2024.111540
Received 1 March 2024; Received in revised form 5 May 2024; Accepted 16 May 2024
Available online 21 May 2024

harvester to prevent spring damage from railway track vibration. The stopper was designed to restrict the movement of the spring to a displacement of 2 mm for vibrations exceeding 2 g acceleration [6]. Three types of shock-absorbing stoppers, each with different levels of flexibility (rigid, parylene-covered and flexible) were proposed and tested on MEMS electret-based harvesters to compare the protecting performance [7]. With a different approach, Chen et al. [8] employed nonlinear air damping as a soft stopper for MEMS piezoelectric energy harvesters. The damping effect could be controlled by adjusting the air pressure level. Furthermore, a mechanical stopper was introduced as a step in the cavity of MEMS piezoelectric energy harvesters aiming to prevent significant stress concentration between the cantilever and the inertial mass, which increased the survival rate of devices [9]. Additionally, a computationally efficient model of the MEMS stopper was created using Comsol software, where the stopper was considered as a rod [10].

Resonant energy harvesters typically exhibit high natural frequencies [11,12], which often do not align with the low dominant frequencies of ambient vibrations, such as those encountered in railway tracks [13], wind-induced vibrations [14], human motions [15], and ocean wave motions [16]. To address this discrepancy, a frequency up-conversion mechanism has been developed by using mechanical impact. As illustrated in Fig. 1(a), an energy harvester with the frequency up-conversion mechanism consists of both resonant and impact systems. Both these systems can be regarded as two separate mass-spring-damper systems. Fig. 1(b) shows the displacement of the two systems subjected to harmonic excitation. In response to a low-frequency harmonic excitation, the resonant system resonates and subsequently engages with the impact system. Following each collision, the impact system freely vibrates at its high resonant frequency, which in turn generates power. This frequency up-conversion mechanism effectively transforms the low-frequency excitation into a high resonant frequency of the impact system. However, it also introduces a new challenge for overload protection. In operation, these harvesters require mechanical impact between the two systems. However, mechanical overloads could make them more prone to damage under a large impact force. Therefore, it is crucial to implement appropriate measures to protect the harvesters from excessive impact force under mechanical overload. A rope design was proposed, which is attached between the two systems. The design limits the displacement of the resonant system, resulting in a 4.2 times increase in frequency bandwidth [17]. Liu et al. [18] utilised a straight cantilever to serve as both the stopper and the impact system, which effectively extended the operation bandwidth by 14 Hz. In another study, Wang et al. [19] introduced an arc-shaped contact surface to prevent large displacements of the cantilever. This design led to enhanced power output and wider operating bandwidth. Similarly, Panthongsy et al. [20] embedded a plastic stopper between the two systems to prevent large displacements of the unimorph cantilever in the impact system, which could cause a crack in the piezoelectric layer. Nonetheless, their analysis was primarily centred on power generation. In general, existing research on mechanical overload protection for harvesters with frequency up-conversion mechanisms focuses on the wideband characteristic of the stopper. There is a lack of research exploring their protection methods, mechanisms, and damping effects.

Consequently, this paper proposes two innovative strategies for mechanical overload protection of energy harvesters with frequency up-conversion mechanisms, targeting both resonant and impact systems. Finite element modelling (FEM) has been used to simulate both proposed protection methods. For verification of the FEM results and refinement of the FEM modelling, experiments have been conducted on an energy harvester with a frequency up-conversion mechanism as a case study. Stress analysis is finally conducted based on the refined model to validate the effectiveness of the protection strategies. The results demonstrated that the proposed stopper and IPC could effectively mitigate the influence of mechanical overload by preventing excessive impact force, which led to a muted growth in the maximum stress and acceleration as the input increased. This confirms the successful implementation of the proposed strategies in protecting the device from mechanical overload.

2. Mechanical overload protection strategies and working principles

Two strategies are proposed to cater to the distinct characteristics of resonant and impact systems individually. Fig. 2 illustrates the relative position of the designed stopper within the resonant system and the impact protection components (IPC) within the impact

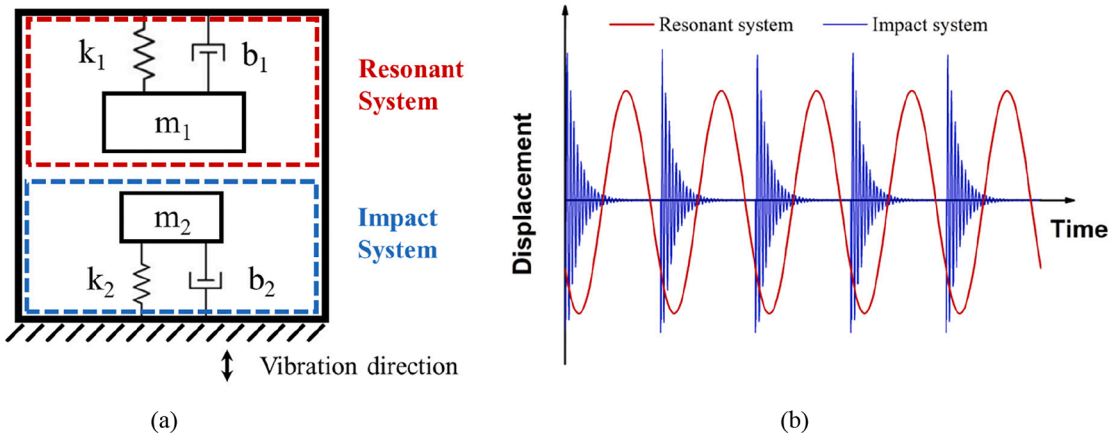

Fig. 1. (a) The schematic of an energy harvester with frequency up-conversion mechanism that uses mechanical impact comprising both resonant and impact systems, and (b) the displacement of resonant and impact systems subjected to harmonic excitation.

system. The detailed configurations of each design will be explained in sections 2.1 and 2.2, respectively. The fundamental aim underlying these strategies is to proficiently minimise the detrimental effects of excessive impact forces that may arise due to high input excitation. Through their implementation, our primary goal is to effectively decelerate the growth of the output maximum acceleration under mechanical overload, thus ensuring the protection of the device.

2.1. Stopper design within the resonant system

Fig. 3 illustrates the proposed design for overload protection in the resonant system and its working principle. The initial state of the system, as depicted in Fig. 3(a), involves adding a stopper beneath the spring at a distance of d_1. Compared to previously reported designs for resonant energy harvesters that utilise a solid plate or rod to impede the motion of the inertial mass, the proposed ring-type stopper features a central hole that permits the inertial mass to vibrate and engage with the impact system below the resonant system. At the same time, the stopper restricts the deformation of the spring when required. During standard excitation, the system operates in the manner depicted in Fig. 3(b), with the spring and inertial mass deforming while maintaining a distance from the stopper. Consequently, the stopper remains inactive, and the energy harvester functions as expected. However, if a large input excitation is applied, posing a risk of damage to the harvester, the stopper comes into play. As shown in Fig. 3(c), the stopper limits the spring's displacement, thereby preventing excessive impact force between the two systems and large acceleration acting on the spring. This mechanism safeguards the energy harvester from mechanical overload, rendering the stopper an effective protective component.

Incorporating a stopper into the resonant system will result in increased spring stiffness and damping coefficient when engaged. The equation of motion can be written as follows according to the impact oscillator equation [21].

$$\begin{aligned} m_1\ddot{x_1} + c_1\dot{x_1} + K_1x_1 + F &= F_e, x_1 < d_1 \\ m_1\ddot{x_1} + c_1\dot{x_1} + c_s\dot{x_1} + K_1x_1 + K_s(x_1 - d_1) + F &= F_e, x_1 \geq d_1 \end{aligned} \tag{1}$$

where m_1 is the inertial mass, x_1 represents the displacement of the plate spring, K_1 and c_1 represent the stiffness coefficient and damping coefficient without the stopper design, K_s and c_s are the stiffness coefficient and damping coefficient caused by the stopper design, F is the impact force, F_e is the excitation force.

2.2. IPC design within the impact system

Another mechanical overload strategy is taken within the impact system to reduce the large impact force and prevent potential

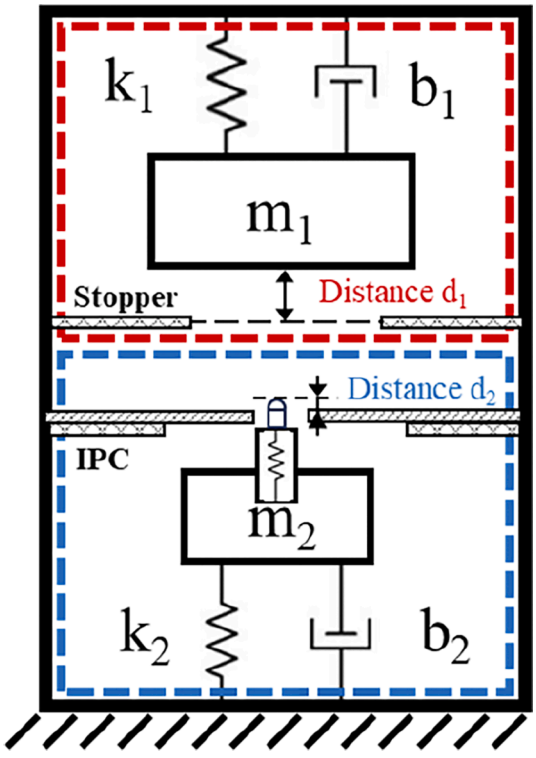

Fig. 2. The relative position of the designed stopper within the resonant system and the impact protection components (IPC) within the impact system.

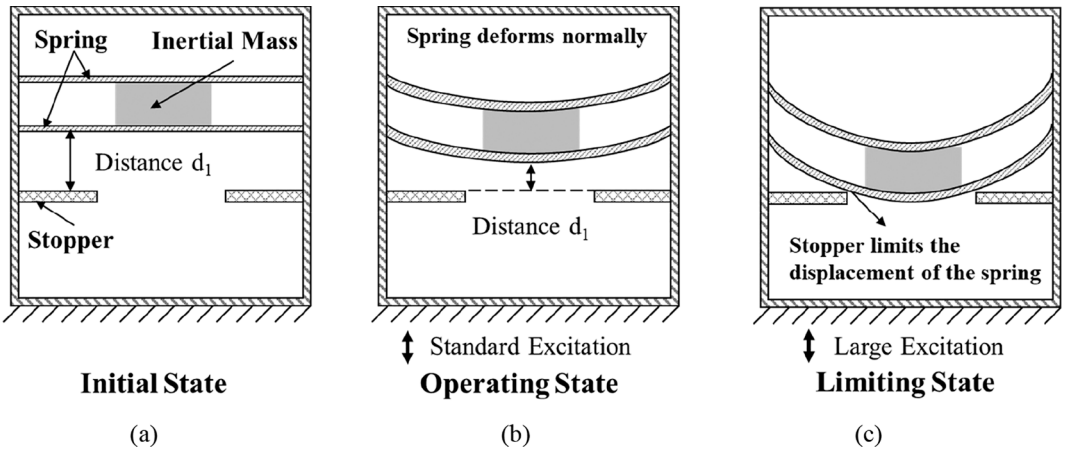

Fig. 3. The proposed design and working principle for overload protection in the resonant system. (a) Initial state, (b) operating state under standard excitation, and (c) limiting state under large excitation.

damage. Fig. 4 depicts the proposed design for overload protection in the impact system and its working principle. In the initial state, as shown in Fig. 4(a), specially designed impact protection components (IPC) are positioned on top of the transducer, comprising a spring, a stopper, and a spring plunger. The spring plunger, a type of encapsulated spring with a bolt or ball plunger, is connected to the transducer. Meanwhile, the spring and the stopper are situated on the base. The spring features a central aperture for the spring plunger's head to protrude. A distance of d_2 separates the head of the spring plunger from the spring. When the impact force is standard, the system operates in the state depicted in Fig. 4(b). The compression spring in the spring plunger gets compressed due to the impact force exerted by the inertial mass, and the energy is transferred to the transducer via the spring plunger. In this state, the head of the spring plunger is pressed down while still being above the spring, and thus the transducer works normally. However, if a large impact force is exerted, as shown in Fig. 4(c), the spring plunger gets further compressed by the inertial mass until it reaches the surface of the spring, where the displacements of the inertial mass and spring plunger's head are limited. In this limiting state, some of the energy is transmitted to the transducer, while the remaining energy is absorbed by the stopper and the base. Consequently, the IPC can effectively protect the energy harvester from mechanical overload.

Incorporating an IPC into the impact system will result in increased spring stiffness and damping coefficient, as well as reduced forced transmitted to the transducer when engaged. Similarly, the equation of the transducer motion can be written as follows.

$$\begin{aligned} m_2\ddot{x}_2 + c_2\dot{x}_2 + K_2x_2 + F(x_2) &= F_e, x_2 < d_2 \\ m_2\ddot{x}_2 + c_2\dot{x}_2 + c_p\dot{x}_2 + (K_2 + K_p)x_2 + F(d_2) + C_r(F(x_2 - d_2)) &= F_e, x_2 \geq d_2 \end{aligned} \tag{2}$$

where m_2 is the mass of the transducer, x_2 represents the displacement of the transducer system, K_2 and c_2 represent the stiffness

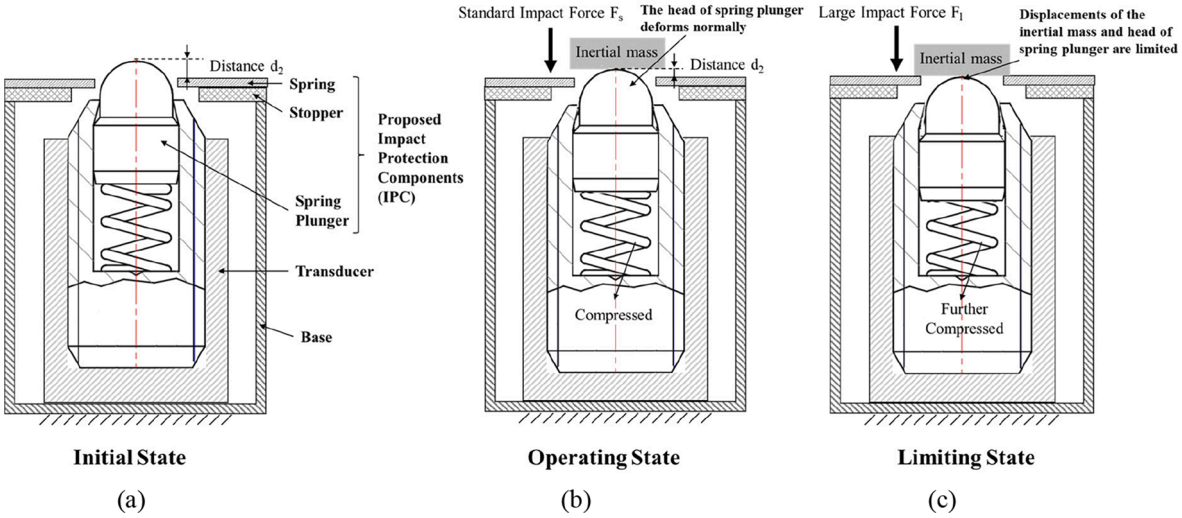

Fig. 4. The proposed design and working principle for overload protection in the impact system. (a) Initial state, (b) operating state under standard impact force, and (c) limiting state under a large impact force.

coefficient and damping coefficient without the IPC design, K_p and c_p are the stiffness coefficient and damping coefficient caused by the IPC design, F is the impact force with regard to the displacement, C_r is the coefficient of damping effects.

3. FEM simulations

To gain comprehensive insights into the protective mechanisms of the proposed methods, modelling analysis is performed using the COMSOL software. An example structure of the energy harvester with a frequency up-conversion mechanism [22] is used in the modelling. The model of the harvester is shown in Fig. 5(a). It consists of two parts, a plate spring structure representing the resonant system, as shown in Fig. 5(b), and a piezo stack transducer that embodies the impact system, as shown in Fig. 5(c).

For the resonant system, an added mass node is introduced to the top of the plate spring to represent the inertial mass. A spring foundation node is used to match the resonant frequency of the harvester in the experiment, while fixed constraints are applied to the four holes of the outer circle. For excitation, a boundary load of harmonic force $F_{harmonic}$ is applied to simulate the harmonic excitation. The resonant system's velocity can be acquired and subsequently applied to compute the impact force using the impulse-momentum principle [23]. This impact force serves as a boundary load F_{impact} for the impact system. In situations where the displacement of the plate spring x_1 exceeds the distance d_1, another spring foundation node with a stiffness coefficient of K_s and a damping coefficient of c_s is added to account for the impact of the stopper.

For the impact system, an added mass node is introduced to the lower layer on top of the transducer to represent the added mass. Fixed constraints are applied to the bottom of the transducer. A periodic triangular force F_{impact} is applied on the upper layer to represent the impact force, and a time-dependent study is used to determine the maximum acceleration output. For the IPC design, A thin elastic layer node with a stiffness coefficient of K_p and a damping coefficient of c_p are applied to the central layer atop the transducer to represent the spring plunger within the IPC design, which serves as a compressive spring interfacing with the upper surface of the impact system. The coefficient of damping effects C_r is applied to the impact force.

3.1. Stopper design

Fig. 6 displays the maximum acceleration for systems with a stopper of 3.5 mm distance d_1 and without a stopper under various boundary loads. For systems without a stopper, the maximum acceleration increases linearly with the boundary load. In contrast, a nonlinear relationship exists between the maximum acceleration and the boundary load for systems with a stopper. The maximum acceleration and its growth rate are the same as that without a stopper when the system is in the operating state. However, when the system enters the limiting state, the growth rate of the maximum acceleration decelerates, indicating the device's protection due to the stopper. Therefore, the stopper is effective in safeguarding the device against mechanical overload, as it helps limit the maximum acceleration in such situations. Furthermore, an increase in the stopper stiffness K_s leads to a decelerated growth rate of maximum acceleration, showcasing an enhanced damping capacity.

3.2. IPC design

Fig. 7 illustrates the maximum acceleration under different boundary loads for systems with and without the IPC, as well as with the spring plunger alone. Simulations are conducted using the IPC of different coefficients C_r with a distance d_2 of 0.5 mm. A coefficient of 0.7 is introduced into the impact force for the system with the IPC design compared to the system utilising only the spring plunger, accounting for the fact that in practice, some energy is still expended by the spring and stopper design due to the relatively short distance d_2. It is noted that the spring plunger within the IPC design has the capacity to magnify maximum acceleration, whereas the spring and stopper components within the IPC design serve to restrain acceleration. Without the IPC, the maximum acceleration has a linear relationship with the boundary load. In contrast, the acceleration of the system with the IPC increases at the same pace as that of the system without the IPC in the operating state. However, in the limiting state, the acceleration of the IPC-equipped system increases at a much slower rate, indicating that the IPC are effective in protecting the transducer from large impact forces. In addition, a decrease

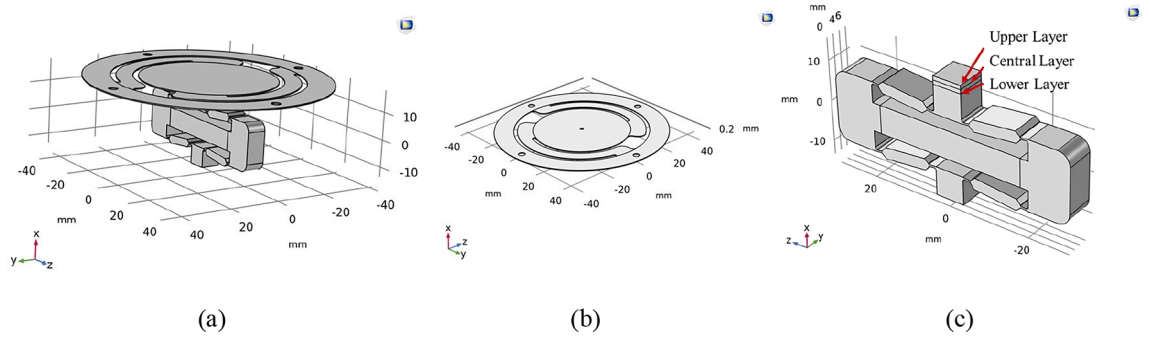

Fig. 5. The FEM model of the example harvester: (a) the whole model of the harvester, (b) a plate spring structure used to model the resonant system, and (c) a piezo stack transducer used to model the impact system.

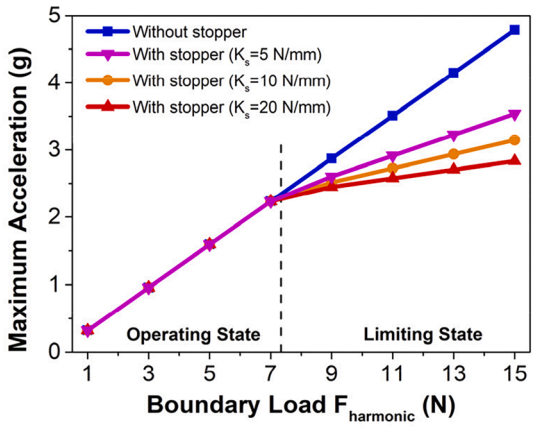

Fig. 6. Simulated results for the resonant system. The maximum acceleration for systems with a stopper of 3.5 mm distance d_1 and without a stopper under various boundary loads.

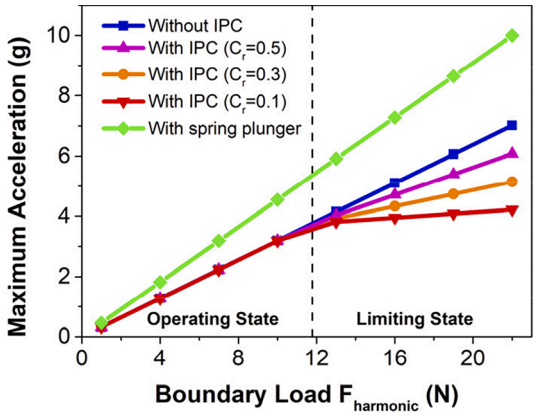

Fig. 7. Simulated maximum accelerations under different boundary loads for the impact systems with the IPC of different coefficients C_r and without the IPC.

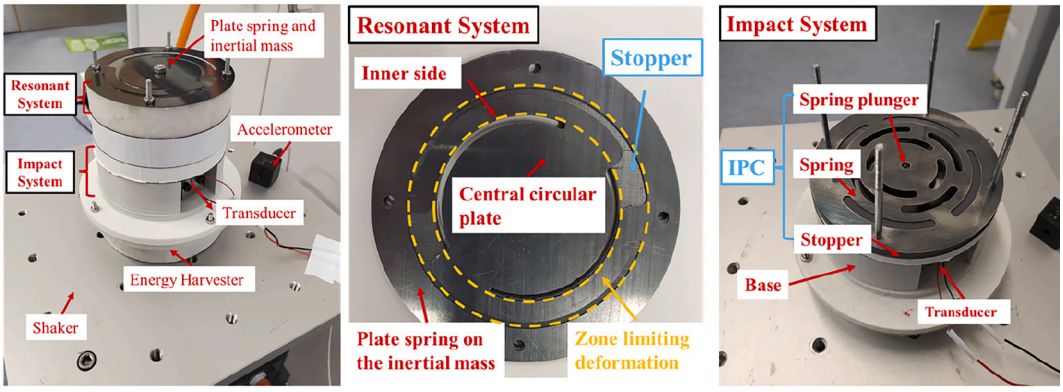

Fig. 8. (a) Prototype energy harvester with frequency up-conversion mechanism comprising the resonant and impact systems, (b) stopper design used within the resonant system, and (c) IPC design used within the impact system.

in the coefficient C_r results in a slower growth rate of the maximum acceleration, demonstrating a greater damping capacity.

4. Experiments

4.1. Fabrication and experimental setup

The proposed protection methods are tested using a prototype generator with a frequency up-conversion mechanism. In Fig. 8(a), the energy harvester consists of both resonant and impact systems. Fig. 8(b) illustrates the design of the ring-type stopper implemented in the resonant system, while Fig. 8(c) shows the IPC design used in the impact system. The detailed design and material of the transducer are listed in Reference [22,24]. The effectiveness of each protection method is tested individually.

In the resonant system, two plate springs and a 0.3 kg inertial mass are used to resonate with low-frequency excitation. A custom-designed stopper made of TPU, known for its exceptional vibration-damping properties, was positioned beneath the bottom plate spring. The stopper's hole diameter was set to match the inner side of the plate spring on the inertial mass. This design allows the central circular plate and the inertial mass to vibrate while restricting the deformation of the plate spring and, ultimately, limiting the impact force and maximum acceleration under large input vibration. There is a distance d_1 between the stopper and the plate spring.

On the other hand, the impact system utilises a piezo stack transducer and a 0.05 kg added mass to generate power from the impact motion. The impact system is equipped with a custom-designed IPC comprising a spring plunger, a spring, and a stopper located on top of the transducer. The spring plunger is screwed into the transducer, while the spring and stopper are situated on the base. The centre of the spring features a hole that allows the spring plunger to protrude. During large input vibration, the spring plunger gets compressed against the spring surface, and further deformation is prevented by the spring and stopper. The spring plunger's head is separated from the spring by a distance d_2.

Fig. 9 illustrates the experimental setup for testing the protection mechanisms of the proposed methods. The configuration consists of a signal generator (Tektronix AFG3022C) providing the input signal, a power amplifier (APS 125) and an electromagnetic shaker (APS 113). The energy harvester and an accelerometer (Kistler 8762A5) are mounted on the shaker. The NI Data Acquisition Card (cDAQ-9174) is employed to obtain both the voltage across the load resistor and the acceleration measured from the accelerometer, which is subsequently recorded in the LabVIEW software.

4.2. Experimental results

4.2.1. Stopper design

In Fig. 10(a), the maximum output acceleration of the energy harvester is depicted with a stopper of 3.5 mm distance d_1 and without a stopper actuated at a resonant frequency of 18 Hz under various input voltage amplitudes. The output acceleration of the harvester without a stopper increases linearly with the input voltage, whereas there is a threshold for the harvester with a stopper. Below the threshold, the input acceleration is standard, and the deformation of the plate spring is lower than the distance, rendering the stopper ineffective. As a result, the output acceleration increases linearly with the input voltage. However, above the threshold, the input acceleration is significant enough to damage the harvester, and the stopper then functions to restrict the deformation of the resonant system. As a result, the maximum output acceleration experiences a slower growth rate, and thus, the stopper effectively

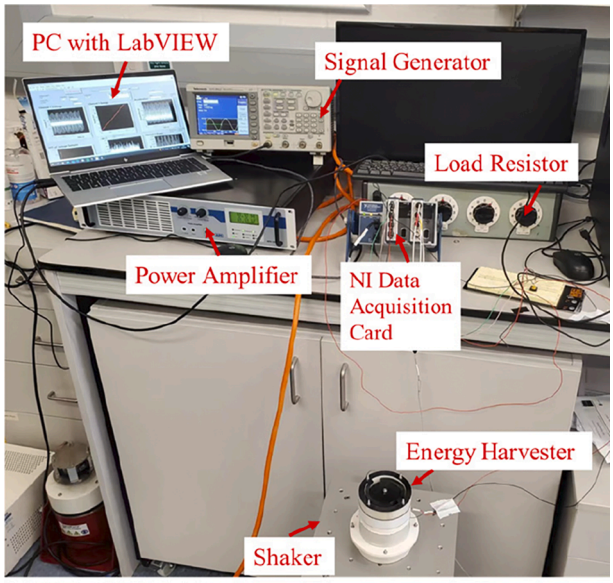

Fig. 9. The experimental setup for testing the protection mechanisms of the proposed methods.

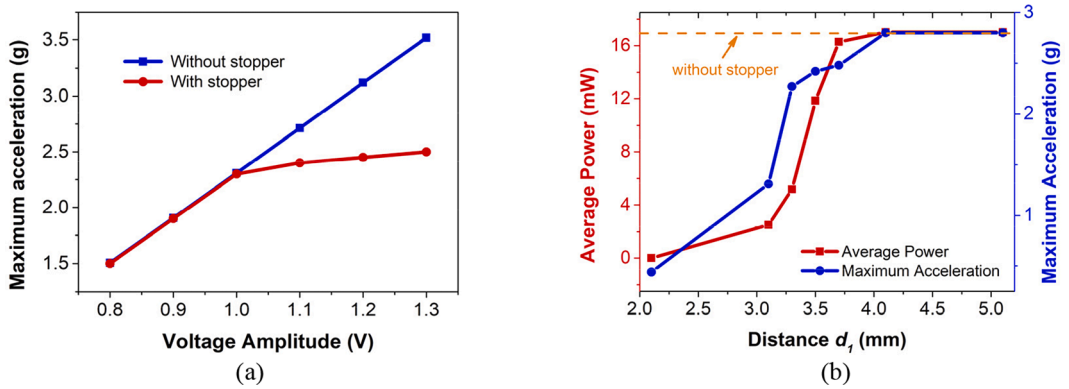

Fig. 10. Measured results for the stopper design. (a) The maximum output acceleration of the energy harvester with a stopper of 3.5 mm distance d_1 and without a stopper under various input voltage amplitudes, and (b) the average power and maximum acceleration with varying distances d_1.

protects the energy harvester from mechanical overload.

Fig. 10(b) displays the average power and maximum acceleration with varying distances d_1 at an input voltage amplitude of 1.1 V. The distance d_1 is adjusted using washers of varying thicknesses between the stopper and the plate spring. Meanwhile, the distance between the resonant and impact systems remains constant to ensure the same initial distance between the two systems. The generated signal from the signal generator and the power amplifier remains unchanged under different d_1. It is discovered that both the average power and maximum acceleration increase with d_1. In other words, a smaller d_1 exerts a more potent damping effect and leads to reduced power. This is because the stopper with a greater distance allows the spring to deform more, resulting in a larger impact force and higher power output. When d_1 exceeds 4.1 mm, the stopper cannot limit the deformation at such acceleration, causing the average power and maximum acceleration to be equivalent to those without the stopper. Thus, different d_1 values can be selected to suit various operating scenarios, considering both the damping effect and the stipulated power output prerequisites.

4.2.2. IPC design

Fig. 11(a) presents the maximum acceleration of the energy harvester under different input voltage amplitudes across various configurations. These configurations include those with and without the designed IPC, along with a configuration that exclusively employs the spring plunger component in place of the entire IPC. The system with the spring plunger component provides valuable insights into the impact of this specific spring plunger element on the system's behaviour. Various washer thicknesses of 0.2 mm, 0.4 mm, and 0.6 mm (corresponding to distance d_2 of 0.5 mm, 0.3 mm and 0.1 mm respectively) are used to adjust the distance between the head of the spring plunger and the spring. A thicker washer leads to a smaller distance for the spring plunger to deform, resulting in further restriction of the maximum acceleration. To ensure the safety of the device, the experimental data points where the maximum acceleration is below approximately 5 g or when the average power reaches around 16 mW are collected and represented as dots. The lines represent the fitted curves based on this data.

The results indicate that the maximum accelerations of the energy harvesters without the IPC and with the spring plunger both increase linearly with the input voltage amplitudes. However, due to the inclusion of the spring component, the system with the spring plunger exhibits much higher maximum acceleration in contrast to its counterpart lacking the IPC. Conversely, when the entire IPC is

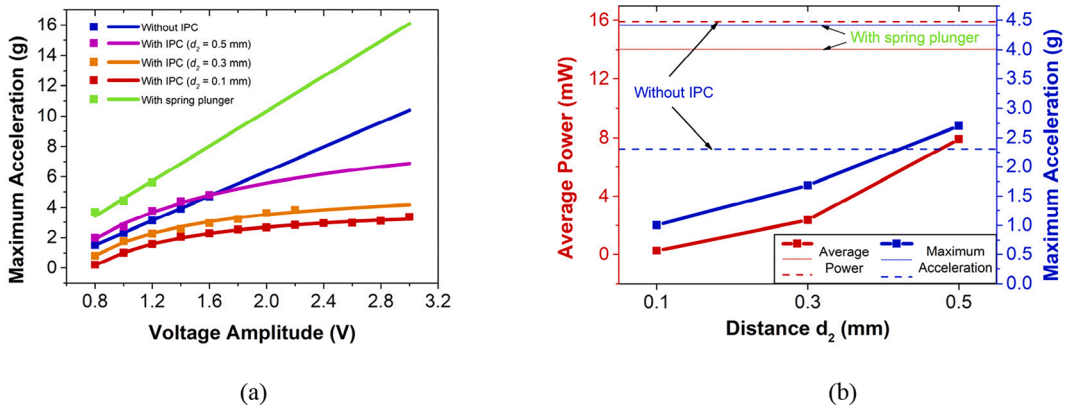

Fig. 11. Measured results for the IPC design. (a) The maximum acceleration of the energy harvester under different input voltage amplitudes across various configurations; the dots represent experimental data, and the lines are the fitted curves according to the data, and (b) the average power and maximum acceleration with varying distances d_2.

present, the system experiences a lower maximum acceleration than when equipped with the spring plunger alone, owing to the constraining role played by the spring and stopper within the IPC.

Furthermore, for the harvester with the IPC, the maximum acceleration growth rate is initially similar to that of the harvester without the IPC. However, As the voltage amplitudes increase, the damping effect becomes evident, resulting in a muted growth in the maximum acceleration. This is because the spring and stopper in the IPC play a greater role in absorbing energy as the voltage amplitudes increase, resulting in a declining proportion of energy being transmitted to the transducer. Consequently, the IPC provides effective protection from mechanical overload.

Fig. 11(b) illustrates the average power and maximum acceleration across varying distances d_2 at an input voltage amplitude of 1 V. The maximum acceleration of the system with the spring plunger alone surpasses that of the system without the IPC due to the amplifying influence of the spring plunger component in the IPC. Meanwhile, it is also higher than that of the system because of the limiting influence exerted by the spring and stopper components within the IPC. It is also observed that the average power decreases correspondingly when adding these components caused by the energy loss. Furthermore, the distance d_2 directly impacts the damping effect and the power output. As distance d_2 decreases, the spring in the IPC becomes closer to the spring plunger, resulting in more energy being consumed by the IPC. Hence, the damping effect becomes more prominent, resulting in a concurrent reduction in maximum acceleration and power output when employing the same input voltage amplitude. Therefore, different distances d_2 can be chosen for different operating conditions, taking into account both the damping effect and the power output requirements.

4.3. Comparison with simulation results

Comparisons between the experimental and simulated results are then conducted to discuss the analysis of the damping effects of the proposed strategies. The relative growth rate of the maximum output acceleration compared to systems without protection methods denoted as β is employed, and calculated as follows:

$$\beta = \frac{B_i - B_{i-1}}{A_i - A_{i-1}}, (i = 2, \cdots, n) \tag{3}$$

where B_i and A_i are the i^{th} output maximum accelerations with and without the protection designs, respectively; n is the total number of data points. A lower relative growth rate β corresponds to a heightened damping effect.

To facilitate refinement of FEM models for subsequent stress analysis, equations (4–6) are derived to obtain the variable stiffness K_s and damping coefficient C_r values by fitting experimental data with simulation data. It is noted that the output maximum accelerations without the stopper (A_s) and IPC (A_r) is proportional to the input acceleration, while the value of K_s and C_r is influenced by the input acceleration. As a result, K_s and C_r are treated as a function of A_s and A_r respectively.

4.3.1. Stopper design

In Fig. 12, the comparison of the growth rate β between the experimental and simulated results with a stopper of 3.5 mm distance d_1 and without a stopper is presented. For simulation, a variable stiffness K_s is used based on the subsequent equation to fit the experimental results, where A_s is the output maximum accelerations without the stopper.

$$K_s = -1713{A_s}^{-4.8225} + 49.9201 \tag{4}$$

The growth rate of the system without the stopper serves as a constant reference. In the presence of a stopper, a distinctive pattern in the behaviour of the growth rate β is revealed. At the operating state, the β value aligns closely with that of the system without a stopper, indicating normal device functionality. As the system transitions to the limiting state, β value exhibits a noticeable decrease as

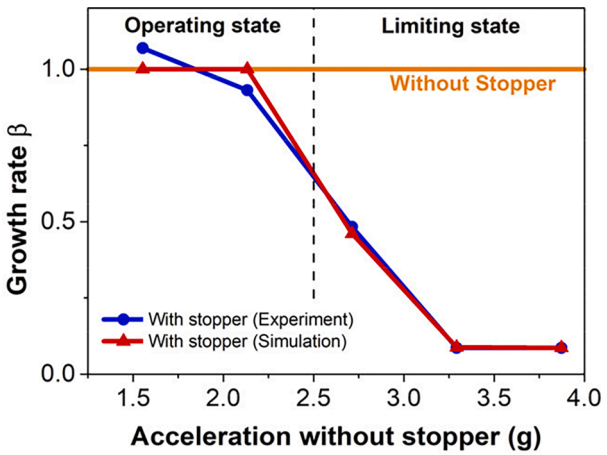

Fig. 12. The comparison of the relative growth rate β between the experimental and simulated results with and without the designed stopper.

the acceleration increases until it stabilises, which means the damping effects become stronger. Notably, this stabilised value is significantly less than that of a system without a stopper in place. This distinct change marks the activation of the stopper, which effectively constrains the relative growth rate of maximum acceleration.

Moreover, it has been observed that the outcomes obtained using variable stiffness closely align with experimental results. This observation underscores the notion that the stopper's stiffness in experimental scenarios exhibits variability and nonlinearity.

In general, the system incorporating a stopper works normally at the operating state and provides protection to the device by limiting the growth rate of the maximum output acceleration at the limiting state. The consistency between the experimental and simulated results further validates the effectiveness of the proposed method.

4.3.2. IPC design

Fig. 13 compares the relative growth rate β between the experimental and simulated results with the designed IPC with 0.5 mm distance d_2 and without the IPC. For simulation, the damping coefficient C_r is calculated below according to the experiment where A_r is the output maximum accelerations without the IPC as C_r is not constant and varies with the input in the experiment.

At the operating state:

$$C_r = -0.9177A_r^{-5.931} + 0.642 \tag{5}$$

At the limiting state:

$$C_r = -0.056A_r^{0.7941} + 0.7838 \tag{6}$$

Likewise, the growth rate of a system without the IPC serves as a constant reference. With the introduction of the IPC, a discernible pattern emerges in the behaviour of the growth rate β. During the operating state, the β value fluctuates around that of the IPC-absent system, signifying the device's regular functionality. As the system undergoes a shift into its limiting state, the β value showcases a noticeable decrease in tandem with the escalating acceleration, and its value is notably lower than that observed in a system without the IPC implementation, demonstrating a significant damping effect. This marked alteration signifies the initiation of the IPC, effectively curbing the relative growth rate of maximum acceleration.

Furthermore, it is noted that C_r first increases in the operating state and then decreases in the limiting state, as the acceleration increases. This is because, in the experiment, a small portion of the energy is still consumed by the IPC in the operating state. As the input acceleration increases, the proportion of energy transmitted to the transducer also increases, resulting in an increase in C_r. In contrast, within the limiting state, the damping effect becomes more and more prominent as the input acceleration increases, resulting in a reduced C_r.

The results indicate that the simulation and the experiment are in good agreement, and the IPC is capable of limiting the growth rate of the maximum output acceleration at the limiting state, thereby protecting the device. Furthermore, a recently explored structure-preserving method offers an alternative perspective to reproduce and analyse the damping effects using the numerical methods [25,26]. In addition, the refined model is employed for stress analysis in the subsequent section.

5. Stress analysis

After verifying and refining the model, stress analysis is subsequently carried out using FEM simulations. These simulations aim to evaluate the impact of the proposed methods on stress levels. Fig. 14 shows the comparison of the maximum stress under various boundary loads $F_{harmonic}$. Four conditions are simulated: without any protection methods, with only a stopper, with only an IPC (Internal Pressure Control) system, and with both a stopper and an IPC system. In order to assess their combined effects, the distance d_1 is adjusted to align the operating and limiting thresholds for both the stopper and IPC design.

It should be noted that in the absence of protective measures, the maximum stress exhibits a linear increase in direct correlation with the boundary load. However, when implementing either the stopper or IPC design, the degree of stress reduction varies. In the case of the system with only a stopper, the maximum stress remains consistent with that observed without any protective measures at the operating state. Nevertheless, the growth rate of maximum stress is noticeably slowed down during the limiting state, resulting in an overall stress reduction.

In contrast, the system equipped solely with an IPC experiences a reduction in maximum stress levels at both operating and limiting states, attributable to the damping effects mentioned earlier. Meanwhile, the growth rate of maximum stress during the limiting state gradually slows down as C_r decreases slowly.

When both stopper and IPC designs are combined, the maximum stress level at the operating state remains consistent with that observed when using only the IPC design. However, during the limiting state, the growth rate of maximum stress closely approximates that of the stopper-only scenario. Consequently, this combined approach leads to a substantial reduction in maximum stress levels.

In summary, the utilisation of the proposed protective measures can lead to a substantial reduction in maximum stress levels when subjected to mechanical overload conditions, making them adaptable to various situations. For instance, the stopper design is ideal for scenarios with relatively low excitation levels, effectively shielding the transducer from sudden overload. Conversely, the IPC design is suitable for high-excitation conditions, efficiently dissipating excess energy to safeguard the transducer. Therefore, the proposed methods serve as a robust defence mechanism, providing protection for the device under mechanical overload.

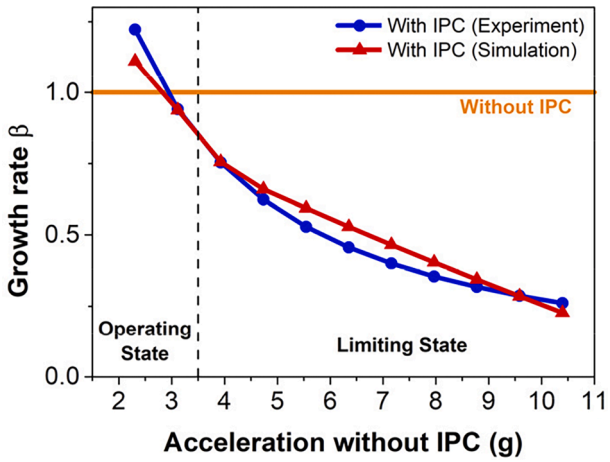

Fig. 13. The comparison of the relative growth rate β between the experimental and simulated results with and without the designed IPC.

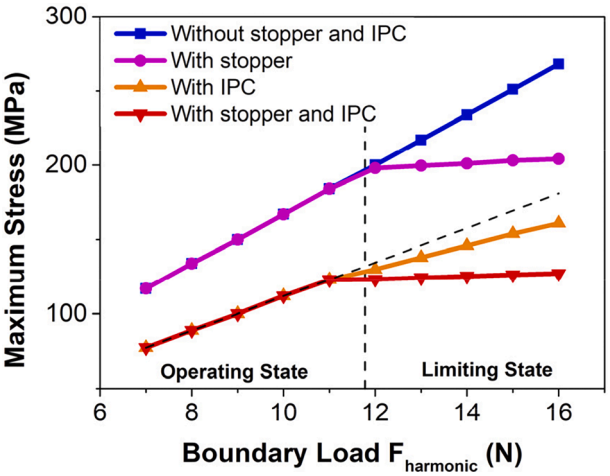

Fig. 14. The comparison of the maximum stress under various boundary loads across different scenarios, including those without any protective measures, with only a stopper, with solely an IPC, and with both a stopper and an IPC.

6. Conclusions

In real-world applications, like railway tracks, bridges, and roads, vibration energy harvesters might have excessive input acceleration applied, potentially damaging the device. This issue is particularly pressing for energy harvesters with the frequency up-conversion mechanism, as they rely on mechanical impacts and are thus more vulnerable to damage under mechanical overload. Therefore, there is an urgent need to find effective methods to protect the energy harvesters from mechanical overload. To tackle this problem, this paper introduces novel protection strategies for energy harvesters with frequency up-conversion mechanisms. The proposed methods aim to alleviate the impact of high input excitation, thereby enhancing the durability of the device. The effectiveness of the proposed methods and their protection mechanism has been validated through both FEM simulations and experimental tests. In conclusion:

1. Two innovative strategies have been proposed to protect energy harvesters from mechanical overload by working on both resonant and impact systems. A designed ring-type stopper has been introduced within the resonant system. The stopper allows the inertial mass to vibrate and interact with the impact system while simultaneously restricting the spring's deformation when necessary. The other method is an IPC consisting of a spring, a stopper, and a spring plunger employed within the impact system. This IPC effectively redirects some of the excessive energy into the base during mechanical overload. This prevents the entire energy from being absorbed by the transducer, thereby avoiding potential damage.
2. Finite element modelling has been used to analyse both proposed protection methods separately. In the case of the stopper design, the introduction of the stopper leads to a change in spring stiffness. In contrast, for the IPC design, the IPC results in a decrease in

the impact force. The findings from the FEM simulations confirm that both methods can keep the transducer working at normal operation in the operating state, while also protecting the device from excessive input excitation in the limiting state.

3. To further verify the FEM modelling results and refine the FEM modelling, experiments have been conducted using an energy harvester with a frequency up-conversion mechanism as a case study. When the proposed stopper or IPC comes into action, a muted increase in maximum acceleration is observed as the input rises. This demonstrates the capability of the proposed methods to protect the device effectively from mechanical overload.
4. Stress analysis has been carried out based on the refined model. The results demonstrate that the proposed strategies decelerate the growth rate of maximum stress in the limiting state, thereby protecting the harvesting system from excessive input excitations.

In summary, this paper not only successfully addresses a significant issue concerning the durability of energy harvesters with the frequency up-conversion mechanism, but also offers practical solutions that have been thoroughly examined and validated. The proposed strategies for mechanical overload protection could have a profound impact on the research field, enhancing the reliability and durability of these devices in various applications.

CRediT authorship contribution statement

Guansong Shan: Writing – review & editing, Writing – original draft, Visualization, Validation, Methodology, Investigation, Formal analysis, Data curation, Conceptualization. **Dong Wang:** Writing – review & editing. **Meiling Zhu:** Writing – review & editing, Supervision, Resources, Funding acquisition.

Declaration of competing interest

The authors declare that they have no known competing financial interests or personal relationships that could have appeared to influence the work reported in this paper.

Data availability

Data will be made available on request.

Acknowledgements

The authors would like to acknowledge the support of the EPSRC through the Project Zero Power, Large Area Rail Track Monitoring under Grant EP/S024840/1 and also the support of University of Exeter.

References

[1] M. Wischke, M. Masur, M. Kröner, P. Woias, Vibration harvesting in traffic tunnels to power wireless sensor nodes, Smart Mater. Struct. 20 (2011).
[2] M. Peigney, D. Siegert, Piezoelectric energy harvesting from traffic-induced bridge vibrations, Smart Mater. Struct. 22 (2013) 095019.
[3] Z. Li, L. Zuo, G. Luhrs, L. Lin, Y.-X. Qin, Electromagnetic energy-harvesting shock absorbers: design, modeling, and road tests, IEEE Trans. Veh. Technol. 62 (2012) 1065–1074.
[4] J. Brans, T.W.A. Blad, N. Tolou, A review of design principles for improved mechanical reliability of cantilever piezoelectric vibration energy harvesters, 2019 7th International Conference on Control, Mechatronics and Automation (ICCMA), IEEE, 2019, pp. 408-415.
[5] J.-H. Kim, J.-W. Jin, J.-H. Lee, K.-W. Kang, Failure analysis for vibration-based energy harvester utilized in high-speed railroad vehicle, Eng. Fail. Anal. 73 (2017) 85–96.
[6] J. Kim, A Study on the Improvement of the Durability of an Energy Harvesting Device with a Mechanical Stopper and a Performance Evaluation for Its Application in Trains, Micromachines 11 (2020) 785.
[7] M. Renaud, T. Fujita, M. Goedbloed, C. de Nooijer, R. van Schaijk, Shock reliability analysis and improvement of MEMS electret-based vibration energy harvesters, J. Micromech. Microeng. 25 (2015) 104010.
[8] S.-T. Chen, S. Du, E. Arroyo, Y. Jia, A. Seshia, Shock reliability enhancement for MEMS vibration energy harvesters with nonlinear air damping as a soft stopper, J. Micromech. Microeng. 27 (2017) 104003.
[9] M. Renaud, Z. Wang, M. Jambunathan, S. Matova, R. Elfrink, M. Rovers, M. Goedbloed, C. De Nooijer, R. Vullers, R. van Schaijk, Improved mechanical reliability of MEMS piezoelectric vibration energy harvesters for automotive applications, 2014 IEEE 27th International Conference on Micro Electro Mechanical Systems (MEMS), IEEE, 2014, pp. 568-571.
[10] T. Peng, Z. You, A Computationally Efficient Model of MEMS Stopper for Reliability Optimization, 2021 28th IEEE International Conference on Electronics, Circuits, and Systems (ICECS), IEEE, 2021, pp. 1-6.
[11] Y. Wu, S. Li, K. Fan, H. Ji, J. Qiu, Investigation of an ultra-low frequency piezoelectric energy harvester with high frequency up-conversion factor caused by internal resonance mechanism, Mech. Syst. Sig. Process. 162 (2022) 108038.
[12] T. Hao, H. Chunrong, H. Huang, L. Weiqun, Z. Yang, Y. Yuan, Z. Zhang, Low-frequency vibration energy harvesting: a comprehensive review of frequency up-conversion approaches, Smart Mater. Struct. (2022).
[13] V.G. Cleante, M.J. Brennan, G. Gatti, D.J. Thompson, On the target frequency for harvesting energy from track vibrations due to passing trains, Mech. Syst. Sig. Process. 114 (2019) 212–223.
[14] T. Tan, X. Hu, Z. Yan, Y. Zou, W. Zhang, Piezoelectromagnetic synergy design and performance analysis for wind galloping energy harvester, Sens. Actuators, A 302 (2020) 111813.
[15] Z. Lai, J. Xu, C.R. Bowen, S. Zhou, Self-powered and self-sensing devices based on human motion, Joule 6 (2022) 1501–1565.
[16] K. Tao, H. Yi, Y. Yang, H. Chang, J. Wu, L. Tang, Z. Yang, N. Wang, L. Hu, Y. Fu, Origami-inspired electret-based triboelectric generator for biomechanical and ocean wave energy harvesting, Nano Energy 67 (2020) 104197.
[17] J. Zhang, L. Qin, A tunable frequency up-conversion wideband piezoelectric vibration energy harvester for low-frequency variable environment using a novel impact-and rope-driven hybrid mechanism, Appl. Energy 240 (2019) 26–34.

[18] H. Liu, C. Lee, T. Kobayashi, C.J. Tay, C. Quan, Piezoelectric MEMS-based wideband energy harvesting systems using a frequency-up-conversion cantilever stopper, Sens. Actuators, A 186 (2012) 242–248.
[19] C. Wang, Q. Zhang, W. Wang, J. Feng, A low-frequency, wideband quad-stable energy harvester using combined nonlinearity and frequency up-conversion by cantilever-surface contact, Mech. Syst. Sig. Process. 112 (2018) 305–318.
[20] P. Panthongsy, D. Isarakorn, P. Janphuang, K. Hamamoto, Fabrication and evaluation of energy harvesting floor using piezoelectric frequency up-converting mechanism, Sens. Actuators, A 279 (2018) 321–330.
[21] B. Tian, S. Yin, Y. Liu, J.L. Monsalve, Nonlinear characteristics identification of an impact oscillator with a one-sided elastic constraint, J. Sound Vib. 575 (2024) 118270.
[22] G. Shan, D. Wang, Z.J. Chew, M. Zhu, A high-power, robust piezoelectric energy harvester for wireless sensor networks in railway applications, Sensors and Actuators A: Physical, (2023) 114525.
[23] G. Shan, M. Zhu, A piezo stack energy harvester with frequency up-conversion for rail track vibration, Mech. Syst. Sig. Process. 178 (2022) 109268.
[24] G. Shan, Y. Kuang, M. Zhu, Design, modelling and testing of a compact piezoelectric transducer for railway track vibration energy harvesting, Sens. Actuators, A 347 (2022) 113980.
[25] W. Hu, M. Xu, F. Zhang, C. Xiao, Z. Deng, Dynamic analysis on flexible hub-beam with step-variable cross-section, Mech. Syst. Sig. Process. 180 (2022) 109423.
[26] W. Hu, X. Xi, Z. Song, C. Zhang, Z. Deng, Coupling dynamic behaviors of axially moving cracked cantilevered beam subjected to transverse harmonic load, Mech. Syst. Sig. Process. 204 (2023) 110757.